Pre-launch status of the Planck mission

Astronomy & Astrophysics

Special feature

Planck pre-launch status: The optical architecture of the HFI

P. A. R. Ade[1], G. Savini[1,2], R. Sudiwala[1], C. Tucker[1], A. Catalano[3], S. Church[4], R. Colgan[5], F. X. Desert[6],
E. Gleeson[5], W. C. Jones[7,8], J.-M. Lamarre[3], A. Lange[7,9,†], Y. Longval[10], B. Maffei[11], J. A. Murphy[5], F. Noviello[10],
F. Pajot[10], J.-L. Puget[10], I. Ristorcelli[12], A. Woodcraft[13], and V. Yurchenko[5,14]

1. Astronomy and Instrumentation Group, Cardiff University, Cardiff, Wales, UK
2. Optical Science Laboratory, University College London (UCL), Gower Street, WC1E 6BT London, UK
   e-mail: gs@star.ucl.ac.uk
3. LERMA, CNRS, Observatoire de Paris, 61 avenue de l'Observatoire, 75014 Paris, France
4. Department of Physics, Stanford University, Stanford, CA 94305-4060, USA
5. Department of Experimental Physics, National University of Ireland (NUI), Maynooth, Co. Kildare, Ireland
6. Laboratoire d'Astrophysique Observatoire de Grenoble (LOAG), CNRS, BP 53, 38041 Grenoble Cedex 9, France
7. Jet Propulsion Laboratory, California Institute of Technology, 4800 Oak Grove Drive, Pasadena, CA 91109, USA
8. Department of Physics, Princeton University, Princeton NJ 08544, USA
9. Department of Physics, California Institute of Technology, Mail code: 59-33, Pasadena, CA 91125, USA
10. IAS, Institut d'Astrophysique Spatiale, CNRS Université Paris 11, Bâtiment 121, 91405 Orsay, France
11. The University of Manchester, JBCA, School of Physics and Astronomy, Manchester M13 9PL, UK
12. CESR, CNRS, 9 Av. du colonel Roche, BP44346, 31038 Toulouse Cedex 4, France
13. SUPA, Institute for Astronomy, University of Edinburgh, Blackford Hill, Edinburgh EH9 3HJ, UK
14. Institute of Radiophysics and Electronics, NAS of Ukraine, 12 Proskura St., 61085, Kharkov, Ukraine

Received 31 July 2009 / Accepted 21 December 2009

ABSTRACT

The *Planck* High Frequency Instrument, HFI, has been designed to allow a clear unobscured view of the CMB sky through an off-axis Gregorian telescope. The prime science target is to measure the polarized anisotropy of the CMB with a sensitivity of 1 part in 10^6 with a maximum spatial resolution of 5 arcmin ($C_l \sim 3000$) in four spectral bands with two further high-frequency channels measuring total power for foreground removal. These requirements place critical constraints on both the telescope configuration and the receiver coupling and require precise determination of the spectral and spatial characteristics at the pixel level, whilst maintaining control of the polarisation. To meet with the sensitivity requirements, the focal plane needs to be cooled with the optics at a few Kelvin and detectors at 100 mK. To limit inherent instrumental thermal emission and diffraction effects, there is no vacuum window, so the detector feedhorns view the telescope secondary directly. This requires that the instrument is launched warm with the cooler chain only being activated during its cruise to L2. Here we present the novel optical configuration designed to meet with all the above criteria.

Key words. cosmic microwave background – space vehicles: instruments – instrumentation: detectors – instrumentation: polarimeters – submillimeter: general – techniques: photometric

1. Background

The *Planck*[1] High Frequency Instrument (HFI) will use very sensitive bolometric detectors cooled to 100 mK to measure polarisation and temperature anisotropies in the cosmic microwave background (CMB) on all scales larger than ~5 arcmin to an unprecedented accuracy of $T \sim 2 \times 10^{-6}$. It is intended that the sensitivity of the instrument will be limited only by the fundamental limits set by CMB photon noise and the ability to remove astrophysical foregrounds. The anisotropy polarisation signature is required to unambiguously reconstruct the spectrum of primordial perturbations and will enable cosmologists to test models for the origin and structure of the Universe (quantum fluctuations or topological defects) and to constrain the key cosmological parameters defining our Universe to an accuracy of a percent or better in most scenarios.

Planck will be injected into a Lissajous orbit around the 2nd Lagrangian point, L2, of the Sun-Earth-Moon system, which subtends a maximum angle of 15° as seen from the Earth. At this location, *Planck* is able to always maintain its payload pointed towards deep space, shielded from Solar, Earth, and Lunar illumination by its solar array. To scan the whole sky, *Planck* spins on a Sun-pointed axis with its telescope oriented at 60 degrees to it looking away from the Sun. A necessary requirement is that the HFI has sufficient pixels at each frequency in the cross scan direction to ensure complete beam sampling of the sky as the satellite spin axis is stepped in increments of 2 arcmin. With this strategy the whole sky is mapped every 6 months.

HFI will measure the CMB radiation over the frequency bands where contamination from foreground sources is at a minimum and the CMB signal is at a maximum. Emission from foreground contributions (the Galaxy and extra-galactic sources) will be removed from the sky maps by measuring the spectral signature of the sky emission over a wide frequency range. The HFI is therefore a multiband instrument with 6 bands from 100 to 857 GHz. The four lowest frequency bands are spread across the peak intensity of the CMB at frequencies centered near, 100, 143, 217 and 353 GHz, respectively. In all these channels we detect the polarisation signature and for all but the 100 GHz channel we also directly measure total power in some sky pixels to enhance the instantaneous detection of foreground sources. Detectors at the same frequency but different polarisation orientation are arranged to follow each other on the scanning path to allow nearly instantaneous measurements of the Stokes Q and U vectors. The overall sensitivity of HFI to the CMB is therefore determined by the inherent sensitivity of each sky pixel (designed to be close to the photon noise from a 3 K blackbody), the number of crossings of each sky element and the number of sky horns for each channel.

For extraction of the two main foregrounds at these frequencies, galactic dust emission and the infrared galaxy background, the HFI has two additional channels at 545 GHz and 857 GHz. These channels have similar or slightly better angular resolution to the CMB channels and thus enable foregrounds which have spectra which rise steeply with frequency to be identified and removed efficiently. To maintain a beamwidth comparable to that used in the CMB channels we use multi-moded horns. These non-diffraction limited beams thus have increased throughput and give better instantaneous detection of point like sources. Unfortunately such horns scramble the polarisation information so only total power is detected at these frequencies.

The HFI frequencies have been carefully chosen to optimize the detection of clusters of galaxies via the Sunyaev-Zeldovich (S-Z) effect. This effect arises from the Compton interaction of CMB photons with the hot gaseous atmospheres of clusters of galaxies. The S-Z effect is expected to be the dominant secondary distortion of the CMB, but can be separated very accurately from the primordial CMB anisotropies via its unique spectral signature. The bands are set so that the S-Z decrement can be observed in the 150 GHz band, the enhancement in the 353 GHz band and the peculiar velocity extracted using measurements from the S-Z null at 217 GHz. The HFI should detect many thousands of S-Z clusters of galaxies Bluebook (2005), probing redshifts $z \sim 1$. The HFI will also detect many thousands of infrared galaxies. The production of complete near all-sky catalogues of galaxy clusters and infrared galaxies with the HFI are important scientific goals of the *Planck* mission.

The *Planck* sky scanning strategy has been chosen to optimize the redundancy in the data by moving the spin axis by up to 10° from the anti-solar direction. An optimized scanning strategy is essential for detecting, controlling and removing systematic effects which might affect the data. The cosmological results from *Planck* will thus be as free as possible from systematic errors.

In the sections which follow we describe the optical architecture which meets with these scientific drivers to ensure that the spectral and spatial performance is achieved with the highest possible on sky sensitivity. As is evident in the above discussion, in meeting with the science objectives there were many obstacles with conventional receiver configurations which needed to be addressed. Here we outline the design parameters and the novel instrument architecture which we have developed to maximize

the science return for HFI and give representative component and system level data.

2. The *Planck* telescope

To observe simultaneously in six frequency bands with multiple detectors to measure polarisation, total power and ensure that we have cross scan beam coverage as well as sufficient sky pixels to achieve the target sensitivity with some redundancy requires a highly packed focal plane layout. This translates to requirements on the off-axis performance of the telescope to minimize straylight and inherent cross polarisation contributions (Tauber et al. 2010). The highest angular resolution requires full illumination of the telescope from the detector feed horns, whereas very low side lobes require under-illumination of the telescope. Thus the philosophy behind the telescope configuration and the consequent optical layout for the focal plane horns is influenced by a number of specific requirements peculiar to the *Planck* Mission (Tauber et al. 2010).

To minimize diffraction and emission from telescope secondary support struts which add significantly to beam asymmetries and detector thermal loading (loss of sensitivity) it was decided to use an off-axis Gregorian telescope with no support struts in the beam and no other structures (window, field stops or filters) in front of the sky horns which directly view the secondary. The *Planck* submillimetre telescope is thus a simple off-axis Gregorian design with two elliptical reflectors providing a 1.5 m projected diameter. Although the performance of this a-planatic configuration is not as good at the field center as a Dragone-Mizuguchi Gregorian (Dragone 1978) configuration which eliminates astigmatism, it is significantly better over the large focal surface required to accommodate the distributed HFI and LFI feeds. The design ensures that there are no support structures in the beam, which could otherwise cause diffraction of the sky beam or radiate unwanted power to the detectors. The emissivity of the telescope is expected to be <0.5%, which with passive cooling to <60 K will minimize the thermal power radiated to the HFI detectors (see Sect. 3.5). Optically the telescope system is equivalent to a single parabolic mirror with an effective focal length of 1.8 m, which focuses the sky radiation onto bolometric detectors located inside the HFI module.

To measure anisotropies at a level of 10^{-6} of the CMB emission there needs to be stringent control of the beam side lobe response. To achieve this demanding criterion the telescope mirrors must be significantly under illuminated by the detector horns. Therefore, the mechanical surface errors of the reflectors are limited to ~ 7.5 μm (rms) near the center and are allowed to increase to ~ 50 μm (rms) near the edge. These surface accuracies provide an optical system with an equivalent wavefront error within ~ 30 μm and ~ 60 μm (Tauber et al. 2010). The carbon fibre reinforced plastic (CFRP) reflectors are coated with aluminium to assure high (>0.995) reflectivity at the operating frequencies. Detailed information on the telescope can be found in Tauber et al. (2010).

Figure 1 shows a schematic of the telescope optics for a few pixels across the focal plane. Two points are important to note here. First, the detectors need to be located on a confocal plane such that each sky horn set (back-to-back horn pair plus detector horn) is appropriately tilted to view the secondary mirror. Secondly, the off-axis focal positions form a tilted curved surface across the focal area as shown in Fig. 2. It is therefore important to ensure that the focus for each pixel is correctly positioned at the phase center of the respective front horn. It is also clear that the variations in focus position needed to be evened
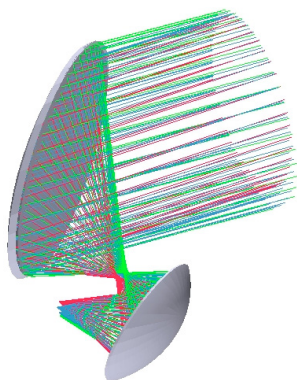
Fig. 1. Sketch of the ray tracing of the *Planck* telescope mirrors for a few pixels.
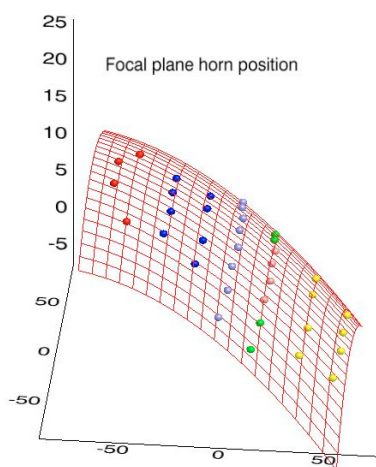
Fig. 2. The curved focal surface of the *Planck* telescope showing HFI pixel locations.

out to enable a single horn mounting surface for all the pixels in the focal plane for mechanical support and thermal cooling to 4 K. Further, since the low frequency pixels use larger and therefore longer horns (scaled with wavelength) careful consideration had to be given to the placement of these channels to avoid shadowing of the much shorter high frequency horns. The final architecture is given later.

Detail of the optical image quality across the focal plane will be found elsewhere (Maffei et al. 2010).

3. The optical architecture of the HFI

The major instrument sensitivity drivers are as follows:

- we need as many sky pixels as possible to maximize the on sky sensitivity;
- we need several CMB channels to spectrally remove foregrounds from dust (largely galactic), synchrotron (radio galaxies) and S-Z clusters;
- we need polarisation sensitivity to remove degeneracies in the determination of cosmological parameters;
- we need to ensure that we get complete cross scan sky coverage and some redundancy in all sky channels;
- we need to identify and remove sub-millimetre foreground sources from the maps.
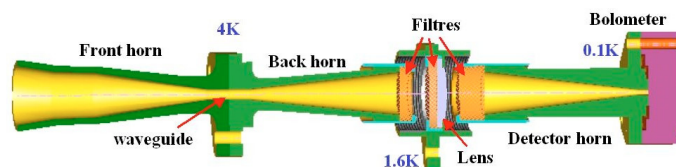
Fig. 3. Single pixel schematic. *From left to right*: photons enter the front-back corrugated horn pair. They encounter the first filter stack (orange) and then exit the 4 K stage and encounter the 1.6 K assembly consisting of astraylight baffle mounting an anti-reflection coated polyporpilene lens (white) for the single-mode pixels with single filter (orange). The 0.1 K filter stack defines the band edge and the detector horn (*right*) couples the photons to the detector in the detector cavity (purple).

These requirements have to be effected within the following constraints:

- the heat lift available at 100 mK was stated to be 150 nW (Bluebook 2005). This needed to include estimates for the in-band optical load, parasitic losses through conduction along the detector readout wires, the cooler tube supports and radiation exchange between the stages;
- the focal surface as shown in Fig. 2 is tilted and curved with the best beam definition being close to the center;
- The whole assembly needs to survive a warm Ariane 5 launch with vibration level approaching 50 g at the focal plane.

The instrument architecture that evolved to meet with all the requirements is complex.

3.1. Single pixel architecture

First, to meet with the stray light and filtering requirements we chose to use a single pixel architecture developed for a previous instrument concept, FIRE (Church et al. 1996). These authors proposed and tested a three-horn optical configuration which utilises a front back-to-back horn pair to view the sky whilst creating a beam-waist at its output where filters can be placed. A third horn then re-condenses the radiation onto the bolometric detector. Importantly, this arrangement, as shown in Fig. 3, allows the spatial, optical and thermal requirements to be independently optimized to meet with the overall requirements of the HFI.

3.2. Spatial control of the Planck beams

To meet with the low side-lobe requirement (Rosset et al. 2009) it was necessary to use corrugated waveguide horn feeds. The advantages of conical horns are well known (Olver et al. 1994) in that they give good control of the antenna response. However, they are also known to have significant asymmetry with respect to the propagation of orthogonal polarized modes generating elliptical beams on the sky. To minimize this effect we have used scalar corrugated feeds throughout. Design parameters and test data for these horns is detailed in a companion paper (Maffei et al. 2010). To maximize the gain all three horns in the optical chain are corrugated as are the waveguide filters between the back-to-back front horn pair and the waveguide exit into the detector cavity.

The 100, 143, 217, and 353 GHz horns are all single mode designs and so produce coherent diffraction limited beam patterns. However, because of mass restrictions and the limited field

of view in the telescope focal plane, the sizes of the horns had to be minimized whilst maintaining the stray light and angular resolution requirements. This optimisation is discussed elsewhere (Maffei et al. 2010). The baseline design is conservative and requires that the total power outside the main beam decreases from 2% at 100 GHz to 0.7% at 350 GHz. With this design, the contamination caused by the signal from the far side lobes (mostly the galaxy) is negligible.

For these CMB channels the beam patterns on the sky are nearly gaussian and well defined by their full width half maximum and their high-pass spectral filtering is defined by the waveguide section of the back-to-back horn pair.

At higher frequencies the requirement is to maintain a beam width close to 5 arcmin to minimize the number of positional changes of the satellite and to keep the data rate within the available downlink specification. By employing corrugated feed horns the beam control of side-lobes is maintained and by increasing the horn waveguide filter diameter extra propagation modes are allowed modifying the illumination of the antenna to a flatter topped profile. Such a modification (described in detail in Murphy et al. 2001) enhances the throughput and hence instantaneous detectivity to point like sources. Optical filtering of the low frequency side of the 545 and 857 GHz photometric bands is achieved using metal mesh high-pass filters.

3.3. Instrument configuration

A suitable instrument layout then emerges; a single outer shield cooled to 4 K was engineered to mechanically support and thermally anchor the 4 K back-to-back sky horns. This had the advantage that the bolometric detectors, which are sensitive to electromagnetic interference, could be surrounded by a Faraday shield. Inside this is a second radiation shield cooled to 1.6 K using a heat lift point on the dilution cooler. This shield would support a second level of filtering and lenses to reimage the output from the back-to-back horn pairs onto the detector horns. Stray light baffles on this shield, as shown in Fig. 3, would also ensure minimal optical crosstalk. Finally we would have a third stage cooled to 100 mK which supported all the detectors and their feed horns. This stage would be thermally attached to the 100 mK cold head.

This looked simple but there are two major issues. First the optical rays having passed through the focus, presumed to be at the phase center of the sky horn, diverge away from the optical axis so the detectors become more spreadout than the front horns and are all tilted according to their position on the focal plane. Secondly, the focal surface is not a regular conic section but is saddle shaped which implied that a single 4 K plate would be difficult to manufacture and align.

A solution was found by noting the following. The design of a horn could be modified to maintain its beam definition whilst giving some flexibility in its length. A common interface with a dished shape 4 K plate commensurate with the junction between the back-to-back horn pair thus became realisable. By following this philosophy through to the 1.6 K and 100 mK stages we conceived of a mechanical structure that met with our optical and thermal requirements in a compact instrument that would nestle within the LFI. Each of the stages requires sufficient mechanical rigidity to maintain the optical alignment whilst having acceptable thermal conduction. The basic cryogenic architecture is shown in Fig. 4.

The next critical issue was to determine how many pixels of each type we could locate in the central region of the focal plane assigned to HFI (see Fig. 5). Two factors became important; first
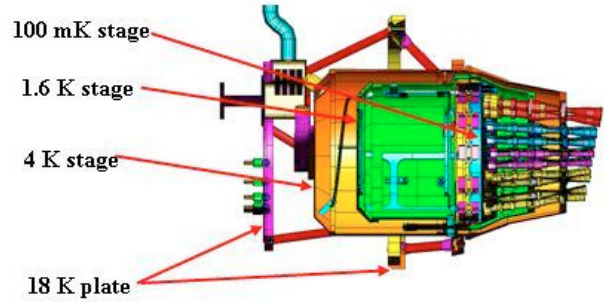
Fig. 4. Schematic of HFI showing cryogenic stages and optical layout. Light blue is 100 mK, green is 1.6 K and orange are 4 K structures.
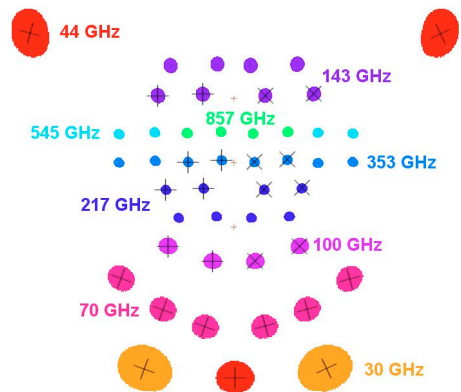

Fig. 5. Schematic of the entrance horns for both HFI and LFI, as seen from the telescope. Lines across horns represent the direction of the measured polarisation, where applicable.

we needed to locate the highest frequencies closest to the optical axis and secondly we needed to make sure that the longer sky horns for the lower frequency bands did not overshadow the shorter high frequency feeds. The saddle shape of the focal surface presented a further complexity to finding a solution.

The overall sensitivity is determined by a combination of the inherent detector noise (photon plus phonon), the number of sky crossings, the number of sky horns and the number of whole sky maps achieved during the mission. Thus the science driver on sky pixel numbers was to pack in as many as we could to maximize the instrument sensitivity. However, there is a thermal constraint on the number of wires allowed to run to the 100 mK stage because of parasitic thermal conductance, and we had a telemetry limit which dictated the number of channels that could be down loaded from the satellite. An additional on-board power limitation also limited the number of detector readouts which we could use. By using a novel capacitive coupled AC readout system (Lamarre et al. 2010), which only requires two wires per detector, we limited the number of wires to the focal plane to enable 52 detector channels to be used. With careful design of the electronics we were able to keep within the on-board power budget.

The location of the different frequency channels in the focal plane is determined by the requirement to minimize the effects of focal-plane aberration and possible horn shadowing from a neighbour. In addition we needed to ensure that a polarisation sensitive bolometer (PSB) detector pair for a given frequency was positioned such that another PSB pair rotated by 45 degrees would follow it on the same scan path. Lastly, in the cross-scan direction, the sky horns need to be staggered to give a sampling step of about 1.5 arcmin, which is consistent with the Nyquist

criterion, and gives a full spatial sampling of the sky for the proposed increments in the satellite spin axis of 2 arcmin. The lowest frequency 100 and 143 GHz beams are large enough to guarantee a correct sampling with the nominal steps in the spin axis. Redundancy is achieved along the scan direction by having two sets of identical detectors (polarized or unpolarized). The selected spectral bands, the number of detectors in each band, their polarisation sensitivity (if any) and the beamwidth of each channel on the sky are given in Table 1.

For the highest frequencies (545 GHz and 857 GHz) the angular resolution requirement does not demand diffraction limited operation for the required spillover levels. Multi-moded horns are therefore used to increase the throughput and coupling to a wider beam on the sky. Multi mode operation is obtained by increasing the wave-guide diameter and allowing higher-order wave-guide modes to propagate. Because of the wide bandwidth the number of modes and, thus, the narrow band-beam pattern will vary across the full 25% bandwidths of the detectors; the integrated pattern has therefore been modelled and measured to ensure compliance with the requirements.

The edge taper and spillover levels for the lower frequency channels have been enhanced through the use of a reflecting baffle positioned around the primary.

The complete cooler chain, which consists of passive radiators to cool to 60 K, H2 absorption to cool to 18 K, a Sterling cooler to reach 4 K and an open cycle He3/He4 dilution system to obtain 100 mK, is described elsewhere (Lamarre et al. 2010). To ensure survival during the Ariane launch the HFI, which consists of three thermally isolated plates containing all the optical components for each frequency, is mechanically locked for an ambient temperature launch. On its cruise to L2 the passive cooling starts and in sequence each cooler is switched on. As low temperatures are reached a thermal mechanical contraction heat switch opens releasing each stage to be held in place by flimsy supports. Parasitic heat loads from the cooler tubes and readout wires were minimized by using a novel dilutor system supported by its own capillary tubes and an ac capacitive coupled detector readout circuit which only required two wires per detector.

To maximize instrument lifetime with limited resources (on board storage of compressed He3 and He4 gases for the dilutor) the available heat lift at 100 mK was limited to ~150 nW. It was thus necessary to stringently minimize the unwanted radiant sky power incident onto the 100 mK detector stage. The solution here was to use heat lift points at 4 K from the Sterling J-T cold stage and at 1.6 K from the dilutor still to sequentially cool the optics chain. In addition the optical filtering was customized to reflect most of the unwanted sky radiant power (all frequencies outside of the HFI bands) back out to the sky. Since complete spectral blocking through to the optical requires 5 individual low-pass filters (Ade et al. 2006) with cutoff edges at successively higher frequencies to prevent harmonic leaks we distributed the radiant load across the temperature stages. Thus the highest frequency rejection filter, which receives the most sky power was placed in a horn cap at the output of the initial back-to-back horn pair which is thermally anchored to the 4 K stage. Next we placed another filter stack to reject lower frequencies at the beam waist between this horn pair and the final detector horn and anchored it to the 1.6 K stage. Lastly, we placed the final band edge defining filters in a horn cap on the detector horn which is anchored to the 100 mK stage. Thus the initial problems of beam definition, optical filtering and temperature loading were resolved by this novel configuration.
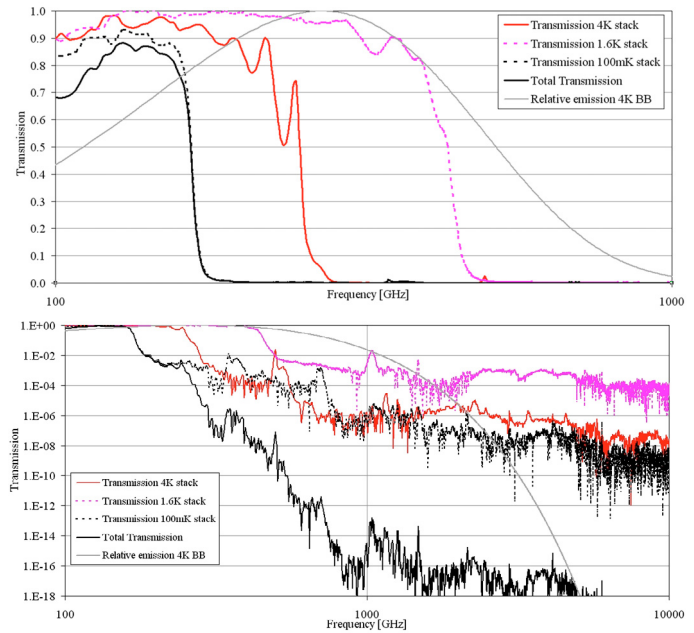
Fig. 6. Spectral transmission of the 4 K, 1.6 K and 100 mK stage filters that constitute the low pass filtering chain of the 143 GHz pixel. Transmission is shown in a linear plot (*left*) and logarithmic plot (*right*). The light grey line in the right plot superimposes the 2.73 K blackbody function.

3.4. Spectral definition of the Planck bands

To maximize the performance of the spectral band defining filters in terms of edge slope and out-of-band rejection they need to be placed at a beam-waist with rays at near normal incidence. This precludes them being placed in front of the sky horn which would have also created addtional side lobe response (Maffei et al. 2010). Placement at the waveguide exit was also considered impractical since these components are optimized for free space impedance matching. The solution was to use a series of three horns (Church et al. 1996) where a front back-to-back pair views the sky and creates a beam-waist at its output where filters can be placed with a third horn condenses the radiation onto the bolometric detector(s) as shown in Fig. 3.

The rejection of unwanted broadband emission from the sky and telescope requires a sequence of filters to guarantee spectral purity in the photometric bands (Ade et al. 2006). Precise definition of the CMB low frequency bands are achieved by using a combination of the high-pass waveguide cut-on between the front back-to-back horns and the low-pass metal mesh filters. It is the precise determination of the waveguide diameter and the geometric parameters of the edge defining low-pass filter which determines the shape, width and position of each band. Because of the requirement to minimize harmonic leaks and achieve a graded rejection of higher frequency radiation as shown in Fig. 7, we use four additional low pass edge filters with staggered low-pass cut-off characteristics. This scheme allows for some flexibility where the unwanted thermal power is dumped as these filters can be placed at either 4 K on the back of the back-to-back horn pair, at 1.6 K or at 100 mK on the front of the final detector horn as shown in Fig. 3. This distribution of filters enables the thermal loading on the three photometer cryogenic stages to be minimized.

The measured spectral performance of the filter stacks on the three stages is shown in Fig. 6 for the 143 GHz band along with the overall low pass filtering performance. The dotted curve in

Table 1. Channel spectral performance.

Channel Label	100	143U	143P	217U	217P	353U	353P	545	857
Centre Freq. (GHz)	101.0	143.6	142.3	221.7	219.2	361.3	359.3	556.3	863.1
Centre Freq. Dispersion σ(GHz)	0.58	0.56	0.71	0.33	0.38	2.29	2.02	1.57	5.36
Upper band egde (GHz)	118	166	163	253	253	411	408	641	992
Lower band egde (GHz)	85	121	121	189	182	306	306	467	734
Average filter transmission over 30% bandwidth (GHz)	0.81	0.83	0.83	0.79	0.79	0.79	0.79	0.57	0.54
No. of unpolarized detectors	0	4	4	4	4	4	4	4	4
No. of lin. pol. detectors	8	0	8	0	8	0	8	0	0
Bandwidth (GHz)	29.8	43.8	42.1	60.6	63.5	95.7	91.9	165.9	248.8
Bandwidth Dispersion σ(GHz)	1.4	0.4	1.4	1.6	1.0	4.4	7.1	3.1	8.1

Notes. Beamwidths listed are from the original design specification. Expected beam characteristics from calibration campaign can be found in detail in Maffei et al. (2010).

Fig. 6 is the intensity radiated by the 4-K filter stack towards the inner system. This emission is determined from knowledge of the filter stack thickness and the measured absorption of the filter polypropylene substrate material. By summing the actual emission for each filter stack for all the channels we determine that the optical power absorbed by the 1.6 K stage is 59 pW. A simple radiative transfer approach can also be used to determine how much power is transmitted through the 1.6 K filter stack to the 100 mK stage. Our estimate is 220 pW which is much lower than the 150 nW of heat lift available from the dilution system.

Spectral characterisation of the HFI instrument was achieved using an external Fourier-transform spectrometer feeding through a polyethylene vacuum window into the integration cavity of the Saturne calibration facility (Pajot et al. 2010). These data were referenced to a calibrated He3 cooled bolometer also viewing into the integrating sphere. Data taken with the HFI detectors allowed recovery of the spectral performance of each pixel referenced to the calibrated bolometer which provides good data above the 1% detection level around the passband. Importantly these data contain the actual spectral transmission of all the optical elements in the HFI photometer (horns, filters, WG cutoff and the detector spectral response) and thus accurately reflect the spectral performance of each HFI detection channel. The multiplied component level data for the horns and quasi-optical filters matches this overall measured performance to good accuracy but lacks in detail on interference effects within the horn-filter-detector assembly.

To determine the out of band response we found that the component level data for the horn WG and metal mesh filters better determined the rejection level since the individual data could be measured to 1:10^4 and hence on multiplication stack rejections could be determined to a level of 1:10^{20}. The best spectral response data is therefore a combination of actual calibration data in the proximity of the passband with concatenated component level data to determine the out of band rejection over an extended frequency range (radio-UV) as shown in Fig. 7. These data show that the out-of-band rejection criteria are easily met.

From the above measurements we arrive at the final instrument parameters for HFI. Table 1 identifies the average spectral band measured parameters (central band frequency, low and high frequency cut-off points defined as position of transmission half-maximum. An idea of the variations on these average values is given by the dispersion also listed in the same table.

These data show that the spectral selectivity of each channel is sufficient to avoid contamination from any out-of-band spectral emission. It should be noted that given the broad spectral response of each channel that cross calibration between
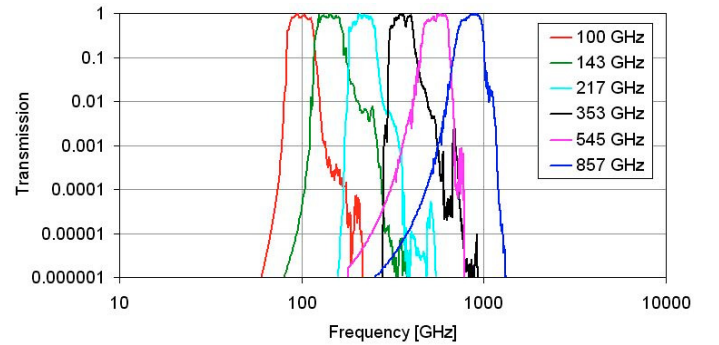
Fig. 7. Averaged normalized spectral response of HFI channels. These data are a combination of calibration data (above 1% level) and component level data (below 1% level).
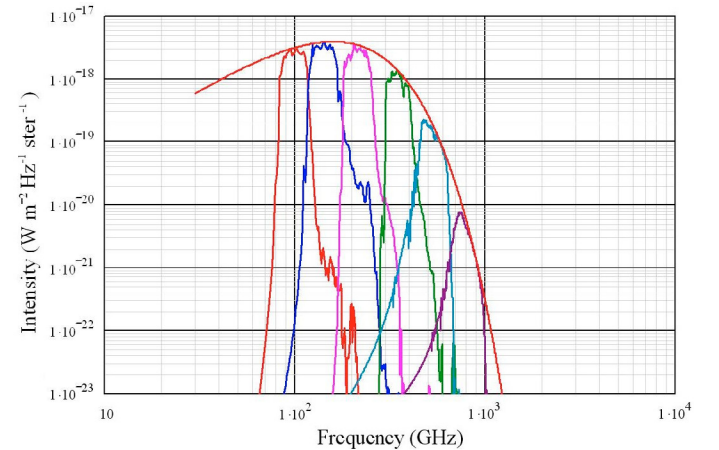

Fig. 8. The product of the spectral bands with the CMB spectrum details the importance of out of band rejection for component separation.

different spectral source types will require spectral corrections as will cross calibration between extended sources (CMB dipole) and point like sources (Planets).

3.5. Thermal loading considerations

Thermal modeling of the power reaching the detector showed that the band edge defining filter needs to be at 100 mK to minimize out-of-band emission from the 4 K and 1.6 K stages reaching the detector. This model also shows that the high pass waveguide filter in the detector horn is necessary to reduce the out of band emission from the 1.6 K and 4 K stages. For the non-CMB channels the high-pass mesh filters and the low pass edge definer
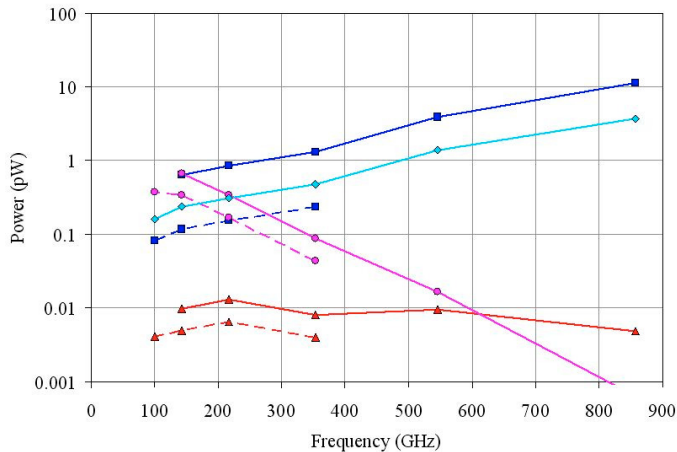
Fig. 9. Plot of thermal optical loading for the different spectral bands. The red line is the loading due to the emission of the warmer stages of the optics and pink is the loading from the CMB emission. Dark and light blue are respectively the loading contribution from the telescope at the nominal (60 K) and expected (45 K) temperature. Dotted lines represent the same for the polarisation sensitive detectors.

both need to be at 100 mK to minimize out of band power at the detectors. The other edges are placed at 1.6 K and 4 K to distribute the power loading in accordance with heat lift margins.

The target was to cool the telescope using passive technology to a temperature below 50 K such that the photon noise from the primary and secondary mirrors with an assumed <1% emissivity would be less than the photon noise from the CMB. This is achieved in the lowest frequency bands where the CMB power peaks. Above this frequency the telescope emission dominates and limits our instantaneous detectivity. Using the radiometric model developed for the filters above we can now identify the power components arriving at the detector. Figure 9 show the major components; telescope emission, CMB power and 4-K stage re-emission as power received by the detectors. It is immediately apparent that thermal emission from the radiatively cooled telescope is dominant in all but the lowest frequency channels. We have shown two situations based on our best knowledge of the *Planck* system; the first is conservative with a 60 K telescope with 1% emissivity and the second represents a goal for a 45 K telescope with 0.5% emissivity. We expect the real system to lie between these limits. The science consequence is not large as we are already CMB photon noise limited in the lowest frequency channels so would gain at most $\sqrt{2}$ in the others if the telescope emission is lower. Significant advances on this will require a cooler telescope and many more pixels.

3.6. Polarisation capability

To measure temperature and polarisation (Stokes *I*, *Q* and *U* vectors) we employ novel polarisation sensitive bolometers,

PSBs (Jones et al. 2003), behind the CMB sky horns which simultaneously detect the orthogonal polarisations. The PSB uses two separate polarisation sensitive absorbers in a single detector cavity. The first bolometer is made of absorbing parallel strips terminated at a single point to the side of the cavity where the detector sensing element is placed. Since there is little loss for transmission of the orthogonal component a second parallel strip absorber, orientated at 90 degrees to the first, can be placed immediately behind it. Thus the PSB concept enables simultaneous detection of orthogonal modes from one sky horn. Use of a second pair of PSBs in a pixel which tracks behind the first pair but with 45 degree orientation to it then enables near simultaneous extraction of *Q* and *U* with some redundancy. The use of corrugated single mode horns is important here as they maintain the polarisation orientation through the three horn and waveguide sections. To ensure that there is no polarisation rotation in the metal mesh filters we have also performed spectral cross polarisation measurements of typical low and high pass filters and have found that there is no measurable component above the 30dB level.

4. Summary

Thus the adopted focal plane architecture which complies with all the requirements is arrived at. It is novel and complex but does meet with the very demanding criteria which the science demands.

We have outlined the design characteristics and optical performance of the *Planck*-HFI. This instrument has unmatched control of its spectral and spatial response as a result of its unique optical configuration. The performance is referenced both to the scientific requirement set and where possible optical modeling.

References

Ade, P. A. R., Pisano, G., Tucker, C., & Weaver, S. 2006, Proc. SPIE, 6275
Bluebook 2005, PLANCK – Scientific Programme, ESA-SCI(2005)1
Church, S. E., Philhour, B., Lange, A. E., et al. 1996, Proceedings of the 30th ESLAB Symposium, ESTEC, Noordwijk, The Netherlands
Dragone, C. 1978, Bell System Tech. J., 57, 2663
Jones, W. C., Bhatia, R., Bock, J., & Lange, A. E. 2003, Proc. SPIE, 4855, 227
Lamarre, J.-M., Puget, J.-P., Ade, P. A. R., et al. 2010, A&A, 520, A9
Maffei, B., Noviello, F., Murphy, J. A., et al. 2010, A&A, 520, A12
Murphy, J. A., Colgan, R., O'Sullivan, C., Maffei, B., & Ade, P. A. R. 2001, Infrared Physics & Technology, 42, 6, 515
Olver, A. D., Clarricoats, P. J. B., Kishk, A. A., & Shafai, L. 1994, IEE electromagnetic waves series, 39, 490
Pajot, F., Ade, P. A. R., Beney, J.-L., et al. 2010, A&A, 520, A10
Rosset, C., Yurchenko, V. B., Delabrouille, J., et al. 2009, A&A, 464, 405
Tauber, J. A., Norgaard-Nielsen, H. U., Ade, P. A. R., et al. 2010, A&A, 520, A2